Proceedings of Australasian Conference on Robotics and Automation, 2-4 Dec 2014, The University of Melbourne, Melbourne, Australia

Background Segmentation to Enhance Remote Field Eddy Current Signals

Raphael Falque[1], Teresa Vidal-Calleja[1], Jaime Valls Miro[1], Daniel C. Lingnau[2] and David E. Russell[2]
[1]University of Technology Sydney, Australia
[2]Russell NDE Systems Inc, Alberta, Canada
Raphael.H.Guenot-Falque@student.uts.edu.au, Teresa.VidalCalleja@uts.edu.au, Jaime.VallsMiro@uts.edu.au,
dlingnau@russelltech.com,drussell@russelltech.com

Abstract

Pipe condition assessment is critical to avoid breakages. Remote Field Eddy Current (RFEC) is a commonly used technology to assess the condition of pipes. The nature of this technology induces some particular noise into its measurements. In this paper, we develop a 3D simulation based on the Finite Element Analysis to study the properties of this noise. Moreover, we propose a filtering process based on a modified version of graph-cuts segmentation method to remove the influence of this noise. Simulated data together with an experimental data-set obtained from a real RFEC inspection show the validity of the proposed approach.

Keywords : Remote-field Eddy-current, Non-Destructive Testing, Image Segmentation, Finite Element Analysis.

1 Introduction

Inspection in pipelines used in water, oil and gas transportation systems is critical to avoid leaks and breakages, which can result in significant damage to the utilities network infrastructure and adjacent properties, expensive repair costs and cause major inconvenience to the public.

Non-Destructive Testing (NDT) sensors are used to estimate the condition along the pipeline. In-line tools provided with this kind of sensors are used to inspect large sections of the pipeline in one go. Examples of NDT sensing techniques include acoustics that measure time-of-flight [Bracken and Johnston, 2009], Magnetic Flux Leakage (MFL) that measure variations in magnetic fields [Edwards and Palmer, B, 1986], and Remote-Field Eddy-Current (RFEC) that measure both time-of-flight and signal strength of a varying electromagnetic field [Atherton, 1995].

Figure 1: Russell NDE Systems Inc. Sea-Snake in-line tool used to detect pipeline corrosion, pitting, wall thinning and graphitisation.

The RFEC (also known as Remote Field Technique) has the capability of measuring the wall thickness of ferromagnetic pipes, as well as detecting and sizing flaws therein. RFEC in-line tools, such as the one shown in Figure 1, measure the "time of flight" (phase shift) and the signal strength (amplitude) of a signal emitted by an exciter coil and detected by an array of receivers. The exciter field induces strong Eddy currents in the inner walls of the pipe near the exciter. These currents produce their own magnetic fields, which are always in opposition to the exciter field. Defects and anomalies are thus detectable because they interfere with the preferred Eddy current paths and magnetic fields.

In RFEC, the magnetic field travels twice in the pipe wall (as shown in Figure 2) which induces important phase lag and amplitude attenuation. This double diffusion (double through-wall effect) in the pipe wall makes RFEC technique less sensitive in some areas, due to the effect of the exciter present in the measured region.

In this paper, we propose an approach to remove the effect of the exciter, which as we will show through 3D Finite Element Analysis (FEA), it is manifested as a circumferential contribution. An approach for background

segmentation based on graph-cuts, commonly used in computer vision, is employed to remove such circumferential contribution. This approach is validated using both FEA simulations and experimental data obtained from a condition assessment inspection in water pipes using the Sea-Snake RFT tool (Figure 1).

2 Remote Field Technology

As mentioned above, remote field Eddy current is an Eddy current pipe inspection technique [Atherton, 1995] used to estimate the wall thickness of a pipe. The first apparition of the RFEC technology was in the patent of W.R. MacLean in 1951 [MacLean, 1951]. The history and the application field of the RFEC are depicted in [Schmidt, 1989].

2.1 Design of the tools

When the first RFEC tools were introduced, the design contained two single coils separated on the axial direction by more than twice the diameter of the pipe. One of these coils, commonly referred as the 'exciter coil", was used to generate a magnetic field. The second coil was used as a sensor to measure the magnetic field at this distance and used to be called the "receiver coil".

Many improvements have been done on the design of RFEC tools. In [Pasadas *et al.*, 2013] advancements on the receivers which replace the exciter coil were proposed, while [Atherton *et al.*, 1989] focus on a magnetic saturation of the pipe, and [Cardelli *et al.*, 1993] worked on the global design of the tool.

For the tool used in this paper to acquire experimental data, the receiver coil has been replaced by an array of multiple sensors that are positioned circumferentially. 56 receivers give the phase shift and amplitude measurements around the pipe at a given instant. For each cycle of the exciter frequency, a clock is started and the arrival time of the signal at the detector is used to reset the clock. The time interval gives a measurement of the time of flight. The signals acquired are amplified, filtered and digitised on-board the tool.

Odometry readings are integrated with the signal reading to be associated directly with the location of the pipe from where they were taken.

2.2 Behaviour of the magnetic field

In RFEC the exciter coil is driven by a low frequency sinusoidal current generating Eddy currents and a magnetic field. The pipe behaves as a waveguide below the cut-off frequency. The exciter field induces strong Eddy currents in the inner walls of the pipe near the exciter. These currents produce their own magnetic fields, which are always in opposition to the exciter field. At a distance of about three pipe diameters, the field in the pipe wall is stronger than the field within the pipe, and can be detected by receivers positioned in the pipe in this "remote field region" [Lord *et al.*, 1988].

Maxwell equations govern the behaviour of RFEC. A solution of Maxwell equations is possible by considering the magnetic field as a plane wave without losses while propagating in the air and the material of the homogeneous pipe with infinite conductivity.

Given these approximations, the expressions for the magnetic field B and the electric field E can be obtained in a straightforward manner [Stratton, 2007]. The solution for B, well known as the depth skin equation is,

$$B = B_0 e^{-\sqrt{\frac{\omega\mu\sigma}{2}}d} e^{i\left(\sqrt{\frac{\omega\mu\sigma}{2}}d-\omega t\right)}, \qquad (1)$$

with B_0 the amplitude of the magnetic flux, ω the angular frequency, μ, ϵ, σ the electromagnetic proprieties of the medium and d the distance of propagation.

The most important information to extract from this expression is the linear relationship between the log-amplitude of the signal and the distance of propagation, together with linear relationship between the phase of the signal and the distance of propagation.

Also in (1), the first exponential influences the amplitude of the magnetic field, while the second exponential is influencing the phase. When acquired by the receivers, the total distance of propagation of the magnetic field within the pipe is twice the thickness of the pipe (*i.e.* the thickness of the pipe in the exciter coil area plus the thickness of the pipe in the receiver area).

This effect can be observed as well by using the Poynting vector (defined as $S = E \times H$, where H is the magnetic flux) when solving Maxwell equations using FEA (without the assumptions made to obtain (1)). Using this operator, [Atherton and Czura, 1991] has shown the effect of the "double through wall", defined as the magnetic field leaving the pipe at the exciter coil location and entering the pipe at the receiver coil location.

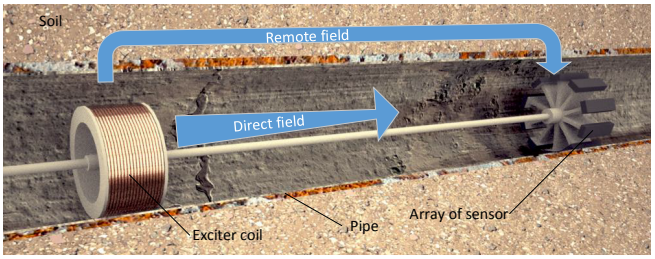

Figure 2: Sketch of a section of a pipe including the RFEC tool showing the path of the magnetic field. The amplitude of the direct field is reduced by the eddy current while propagating inside the pipe. The remote field propagates outside of the pipe and goes back inside the pipe in the receiver area.

3 Finite Element Analysis

FEA is a common method to find a solution of the RFEC problem (solving Maxwell equation via finite elements). In this section we used FEA to analyse how the double through-wall effect impacts the magnetic field in the presence of a local defect.

Although 2D FEA is quite efficient and fast to compute, there are two main disadvantages by using a 2D geometry; 1) it is only possible to create a defect along the circumference, 2) the path of the flow of the magnetic field is defined by a plane. On the other hand, by using a 3D geometry, the magnetic field flow along the circumferential axis can be studied. The main disadvantage of the 3D simulations is the high computational complexity and memory requirements due to the large areas that need to be analysed in detail (three times the pipe diameter).

3.1 3D Simulation geometry

In recent years, there have been some efforts to perform 3D FEA of the RFEC using simplifications that allow executing a simulation. [Wu *et al.*, 2009] used two different simulation scenarios combined: the first one to simulate the magnetic field and a second one with a smaller section of the pipe. By using the distribution of the magnetic field acquired from the precedent simulation and a finer mesh, the authors were able to analyse the interaction with the defects of the pipe. In [Nakata *et al.*, 1990] a 3D open-boundary was defined to allow the use of symmetries and the infinite element domain to reduce the size of the geometry.

In this work, we propose to model the pipe as a infinite cylinder and the exciter coil as a small cylinder. A local defect is created on the side of the pipe in order to analyse the behaviour of the magnetic field while it propagates outside of the pipe (see Figure 3). This defect is displaced in the axial direction to simulate the impact on the receiver measurement with the different configurations of the geometry.

We propose to use anti-symmetries for the magnetic field and symmetries for the current in the axial direction. The current symmetries are imposed by defining $\mathbf{n} \times \mathbf{H} = 0$ on the axial boundaries, with $\mathbf{n}$ the normal of the boundary (since the pipe and the exciter coil are modelled by cylinders it is convenient to use cylindrical coordinates) and $\mathbf{H}$ the magnetic field. On the angular boundaries, we set symmetries on the magnetic field by defining $\mathbf{n} \times \mathbf{A} = 0$, where A is the magnetic vector potential.

Using these boundary conditions allows us to create four planes of symmetry, which reduces the size of the geometry by more than 2^4. Moreover, we use an infinite element domain to reduce the radial size of the air-box, which shortens the size of the geometry by a ratio $\propto \rho^2$ with ρ the radius of the air-box. The final geometry used for this simulation is shown in Figure 3.

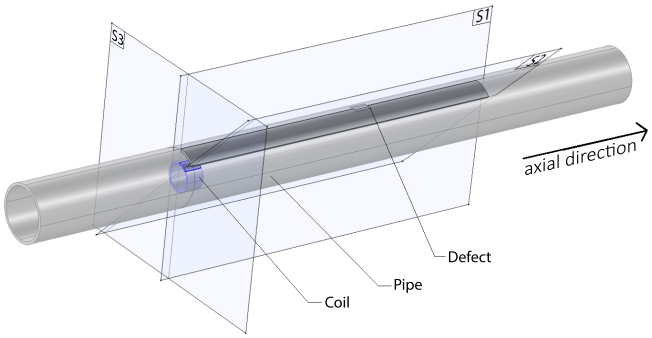

Figure 3: Geometry of the FEA using symmetries on the axial and polar axis (symmetry plans S1, S2 and S3). The exciter coil (in blue) and the pipe (in grey) are model by section of cylinders to reduce the complexity of the computation.

3.2 Output of the simulation

After varying the location of the local defect to three different locations; a) outside the influence of the exciter and receiver, b) on top of the exciter and c) on top of the receiver, the Poynting vector (describe in 2.2) is shown in Figure 4.

As shown in Figures 4a and 4c, the magnetic field behaves in a similar way in both cases with a slight change in the receiver area. However, for a variation of geometry over the exciter coil area, the magnetic field spreads along the pipe as shown in Figure 4b. When the magnetic field reaches the receiver area, it is homogeneous around the circumferential axis. It could then be perceived as a circumferential change on thickness from all the receivers.

In order to generate a set of measurements from the FEA simulation that emulates the output of the experimental tool, we used the location of the defect as a parameter sweep and took an array of measurements (phase shift and amplitude) along the circumferential axis. One hundred simulations were generated at different defect locations from the area of the exciter coil towards the receiver area.

The phase and the amplitude of the magnetic field measured for this parameter sweep are shown in Figures 6 and 5. Note that the pipe has been converted from cylindrical coordinates to Cartesian coordinates, where the Y axis goes along the circumference in all the plots.

According to these results, the contribution of the exciter coil can be considered as a circumferential offset on both phase and amplitude. This behaviour seems logical, as the different parts of the wave going through the pipe in the exciter coil are superimposed while propagating along the pipe. When these waves reach the receiver

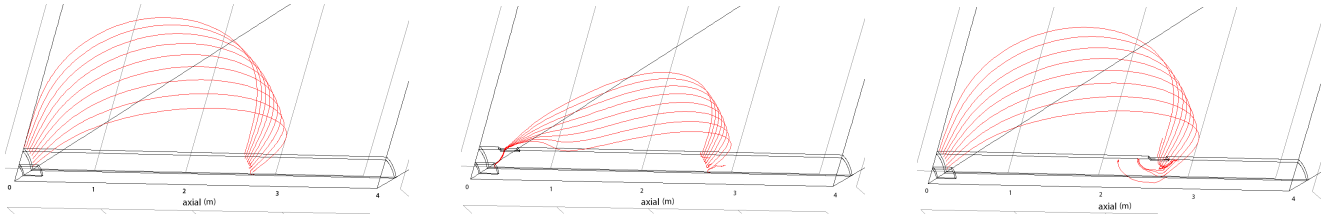

(a) (b) (c)

Figure 4: Plot of the streamline, showing the path of the magnetic field which expand from left to right, in different geometries: there is no defect in (a), a defect is located in the exciter coil area in (b), and in (c) the defect has been moved to the receiver area.

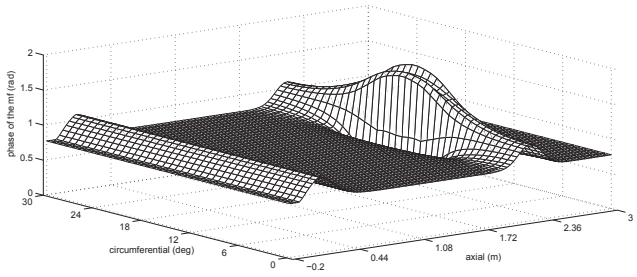

Figure 5: Measurement of the phase of the magnetic field with a sweep on the defect position along the pipe. The first "wave" on the left correspond to the signal while the defect is located in the exciter coil area. The second "wave" is when the defect is located in the receiver area.

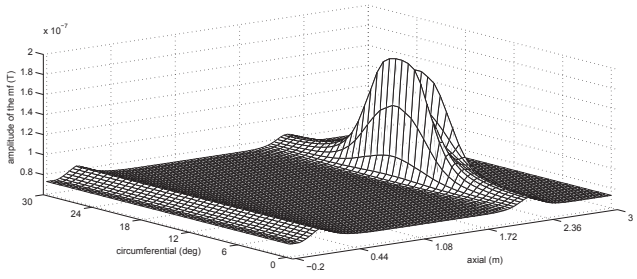

Figure 6: Measurement of the amplitude of the magnetic field with a sweep on the defect position along the pipe.

area they could be considered as plane waves.

Using these simulation results, the RFEC signal can be separated into two distinct parts; 1) the background field, which includes the contribution of the exciter coil, and 2) the defect field which has a direct correlation with the local geometry located near the receivers. Note that estimating the geometry of the local defects is critical to assess the condition of the pipe.

4 Background segmentation

In this section we describe the proposed approach to remove the background field from the RFEC signals in order to obtain signals/images that consider only the defect field and therefore correlate in a direct manner with the real status of the pipe.

Several techniques under different names, according to the research field, to separate the background from the foreground in sensor outputs have been presented in the literature. In computer vision this is commonly referred as image segmentation for 2D images (a survey can be found in [Peng *et al.*, 2013]), or background subtraction for videos as examined in [Mayo and Tapamo, 2009]. In robotics this is commonly referred as background segmentation as is applied to 3D scans to extract the ground such as in [Douillard *et al.*, 2012]. The main difference between these works is the prior assumed to produce an efficient segmentation.

The majority of the work in background segmentation has been applied to 2D images, among the many different methods available thresholding, region growing, histogram based, graph-cuts are the most common. Our approach is based on the graph-cuts method presented in [Felzenszwalb and Huttenlocher, 2004]. This method presents multiple advantages such as speed, efficiency and, more importantly, the ability to handle slow change of intensity, which is needed considering the nature of RFEC signals.

More related to our work and specifically for background segmentation in RFEC is the method presented in [Zhang, 1997], which relies on manually picking two measurement lines as a reference (the measurement lines are defined along the axial direction) that are the most representative of the background. To create the background field, a simple linear interpolation in between each points of the measurement lines is employed. The main downside of this method is the need for a manual intervention.

4.1 Graph-based segmentation

Given the nature of the REFC signal, a segmentation method with a high sensitivity on the circumferential direction to separate the signal with high influences from the defect field is required. We propose a modification of a segmentation algorithm that makes it more sensitive in this direction.

The segmentation algorithm used in this work is based on the graph-cut theory [Felzenszwalb and Huttenlocher, 2004]. This method transforms an image into a graph $G = (V, E)$, with each pixel defined as a vertex $v_i \in V$. Each pixel is link to the pixels in its neighbourhood with edges $(v_i, v_j) \in E$. Where each edge has a weight $w((v_i, v_j))$ that is defined by a positive measurement of the dissimilarity between v_i and v_j.

The pixels V are segmented into components $C \subset V$ according to a decision criteria D defined as:

$$D(C_1, C_2) = \begin{cases} \text{true} & \text{if } \mathrm{Dif}(C_1, C_2) > \mathrm{MInt}(C_1, C_2) \\ \text{false} & \text{otherwise} \end{cases} \tag{2}$$

where the difference is

$$\mathrm{Dif}(C_1, C_2) = \min_{\forall v_i \in C_1, \forall v_j \in C_2, \forall (v_i, v_j) \in E} w((v_i, v_j)), \tag{3}$$

the minimum internal difference is

$$\mathrm{MInt}(C_1, C_2) = \min(\mathrm{Int}(C_1) + \tau(C_1), \mathrm{Int}(C_2) + \tau(C_2)), \tag{4}$$

the internal difference $\mathrm{Int}(C)$ within the Minimum Spanning Tree (MST) as

$$\mathrm{Int}(C) = \max_{e \in \mathrm{MST}(C,E)} w(e), \tag{5}$$

and a threshold function based on the size of the component defined as

$$\tau(C) = \frac{k}{|C|}. \tag{6}$$

Using n as the number of pixels in the image and m the number of edges, Algorithm 1 generates the final segmentation S based on the distance criteria.

In the authors' implementation, the weight is defined for monochrome images as $w((v_i, v_j)) = |I_i - I_j|$. However, to improve the sensitivity of the segmentation on the circumferential direction, we proposed to modify the weight to be inversely proportional to the axial distance,

$$w((v_i, v_j)) = \frac{|I_i - I_j|}{|y_i - y_j| + 1}, \tag{7}$$

with I the intensity of the pixel v and y its circumferential position.

Algorithm 1 Graph-based segmentation

INPUT: $G = (V, E)$
OUTPUT: $S = (C_1, ..., C_r)$
sort E **into** $\pi = (o_1, ..., o_m)$, **by increasing** w
initialisation: create a C_i for each v_i
for q = 1,...,m **do**
  Set i and j from the edge $o_q = (v_i, v_j)$
  if $C_i^{q-1} \neq C_j^{q-1}$ & $w(o_q) \leq MInt(C_1^{q-1}, C_2^{q-1})$ **then**
    merge C_i^{q-1} and C_j^{q-1} in S^{q-1}, $S^q = S^{q-1}$
  else
    $S^q = S^{q-1}$
return $S = S^m$

The signals from the RFEC tool are high resolution on the axial direction (one measurement each 2 mm) and low resolution on the circumferential direction (one measurement each 6.4°). The edges are defined according to a square neighbourhood, the weight will then be higher on the circumferential direction than the axial direction since a higher spatial distance will be covered by the neighbourhood. This property of the images combined with the threshold parameter k leads to high sensitivity of the segmentation on the circumferential direction.

The segmentation is then transformed into a mask M defined as

$$M = \sum (C_i > \frac{n}{20}) \tag{8}$$

which represents the background of the signal. This mask is then composed by the large region that represents the background and small regions that are more likely to be the locals defects.

The background field is then estimated as a circumferential offset, using the average value of the magnetic field within the mask.

The circumferential offset gives us an estimation of the background field. This background field is then subtracted from the magnetic field to obtain the defect field.

5 Evaluation of the approach

In order to show the performance of our approach, we have compared the proposed algorithm with the one proposed by Zhang in [Zhang, 1997]. Simulated and experimental data from an actual inspection are used to evaluate both approaches.

5.1 Simulated data

The FEA simulation presented in Section 3.2 is used to show the performance of our method. The results are presented focusing on the phase of the signal which is displayed on Figure 5.

As mentioned above, the approach proposed in [Zhang, 1997] the two measurement lines of the

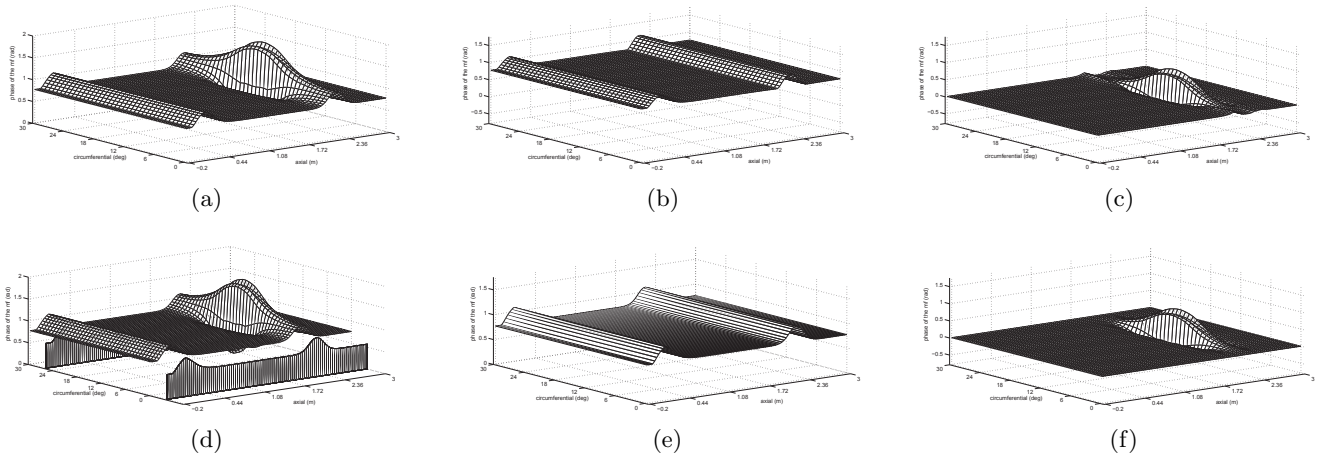

Figure 7: Result of the background removal technique. Our method automatically estimates the background (b) from the full-field (a) and build the defect field (c) by subtraction. For comparison we show the result of the method describe in [Zhang, 1997] where slices representative of the background are extracted manually (d) to estimate the background field (e) and recreate the defect field (f) using the same method.

RFEC signal along the axial direction, which are the most representative of the background (this corresponds to the slices on either side on Figure 7d) are used as a reference to estimate the background field. The background field obtained by linear interpolation of these lines is shown in Figure 7e.

Zhang's method is used as a benchmark, because if the two measurement lines are properly picked, the method will accurately remove the background in simple cases such as this simulated scenario. We use the extracted slides which are shown in Figure 7d as a reference to estimate the background. The background segmentation is shown in 7e and the final result of the defect field extracted with this method is shown in the Figure 7f.

As shown in Figure 7f, this method performs very well on simulated data, but it has several important issues. There is a need to find the measurement lines which are more representative of the unknown background. Moreover the background is estimated using only two measurements, which can lead to a noisy estimation. Finally, the process is time-consuming in particular for large datasets.

The estimated background using our method is presented in Figure 7b and the results of the background extraction is shown in the Figure 7c.

Our method shows similar performance to Zhang's approach on this data, which has the optimal performance in the presence of no-noise. Moreover, our method offers the advantage to be automatic therefore can be applied to large datasets and it is more robust to perturbation as we will show in the results using real data.

5.2 Real data

Experimental data from a 1-km RFEC inspection in a 660mm diameter cast-iron water pipe has been used to validate our algorithm. The raw data has been provided to us in the form of signal phase and amplitude associated to the distance measured by the tool's odometer. The tool used to collect this dataset is shown in Figure 1.

Three pipe sections have been chosen to be extracted due to their poor condition and used as ground-truth. The extracted pipe sections have been processed using a protocol established to get relevant information of their quality. Measurements from the nearest joint along the pipe have been taken to locate the section. The pipes have been cleaned and a 3D profile of the remaining wall thickness has been established using a high-definition 3D scanner as shown in Figure 8. An accurate 2.5D thickness plot has been produced as described in [Skinner *et al.*, 2014].

In order to show the real-data results instead of the

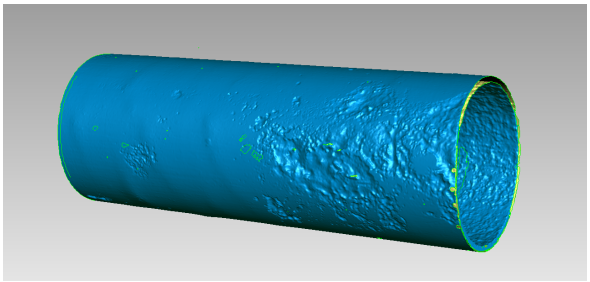

Figure 8: 3D profile of a extracted pipe obtain with a 3D laser scanner.

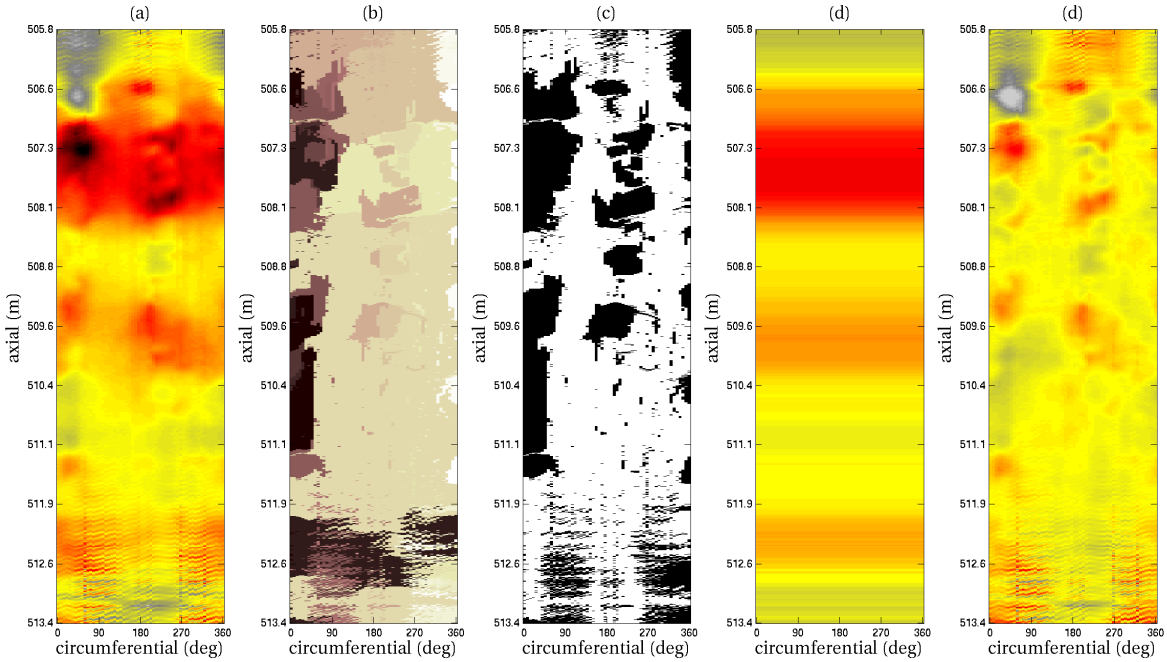

Figure 9: Graph-cut segmentation approach applied to a pipe segment. The full field (a) is transformed into a labelled map of region (b). The region corresponding to the background is then transformed into a background field (c), which is extracted from the full field to obtain the defect field (e).

surface plots used for the simulated data, we opted to use color images where the vertical axis represents the circumferential axis of the pipe, the horizontal axis is along the axial direction and the colour axis represents the magnitude of the signal (in the case of RFEC) and the thickness (in the case of the ground-truth). A spatial normalisation is applied on each image to scale it to the same resolution, which requires interpolation. Using the fact that each image comes from a cylindrical model that has been converted into a two dimensional matrix, when changing the circumferential resolution it is beneficial to create an overlap on the extrema. This method produces a better approximation while interpolating the values located near the edges (which correspond to the overlapping region of the circumferential axis).

More formally, from the original image I of size $r_1 \times s_1$, we define a temporary matrix J of size $r_1 \times (s_1 + 2)$ by:

$$J_{r_1,s_1+2} = \begin{bmatrix} I_{1,s_1} \\ \vdots \\ I_{r_1,s_1} \end{bmatrix} + \begin{bmatrix} I_{1,1} & \cdots & I_{1,s_1} \\ \vdots & \ddots & \vdots \\ I_{r_1,1} & \cdots & I_{r_1,s_1} \end{bmatrix} + \begin{bmatrix} I_{1,1} \\ \vdots \\ I_{r_1,1} \end{bmatrix} \quad (9)$$

To resize the image I_{r_1,s_1} to the size $r_1 \times s_2$ we use a proportion factor α_x on the circumferential axis defined by:

$$\alpha_x = \text{round}(s_2 \frac{s_1 + 2}{s_1}) \quad (10)$$

Table 1: L_1 norm comparison wrt the ground-truth

	raw data	our approach	Zhang's approach
pipe 1	139.8	120.3	124.2
pipe 2	156.2	156.4	156.3
pipe 3	183.0	169.4	174.5

The additional columns created are then deleted to match to size $r_1 \times s_2$.

We then apply the background segmentation to improve the correlation between the real geometry and the RFEC data. Figure 9 shows the result of each step of the segmentation algorithm applied on a pipe length, including the segmentation into different regions (b), the creation of the mask (c) use for the estimation of the background (d) and the result of the final defect-field (e) obtain through this method.

Both RFEC data and ground-truth data are standardised to allow direct comparison of their values within the same range. The result after the normalisation and standardisation processes is shown on Figure 10.

A quantitative evaluation has been done by computing the Manhattan distance Manhattan distance (L_1) between each method and the values of the ground-truth. The result of this evaluation is presented in Table 1. The results in Table 1 show that RFEC signals correlate better with the ground-truth once the background

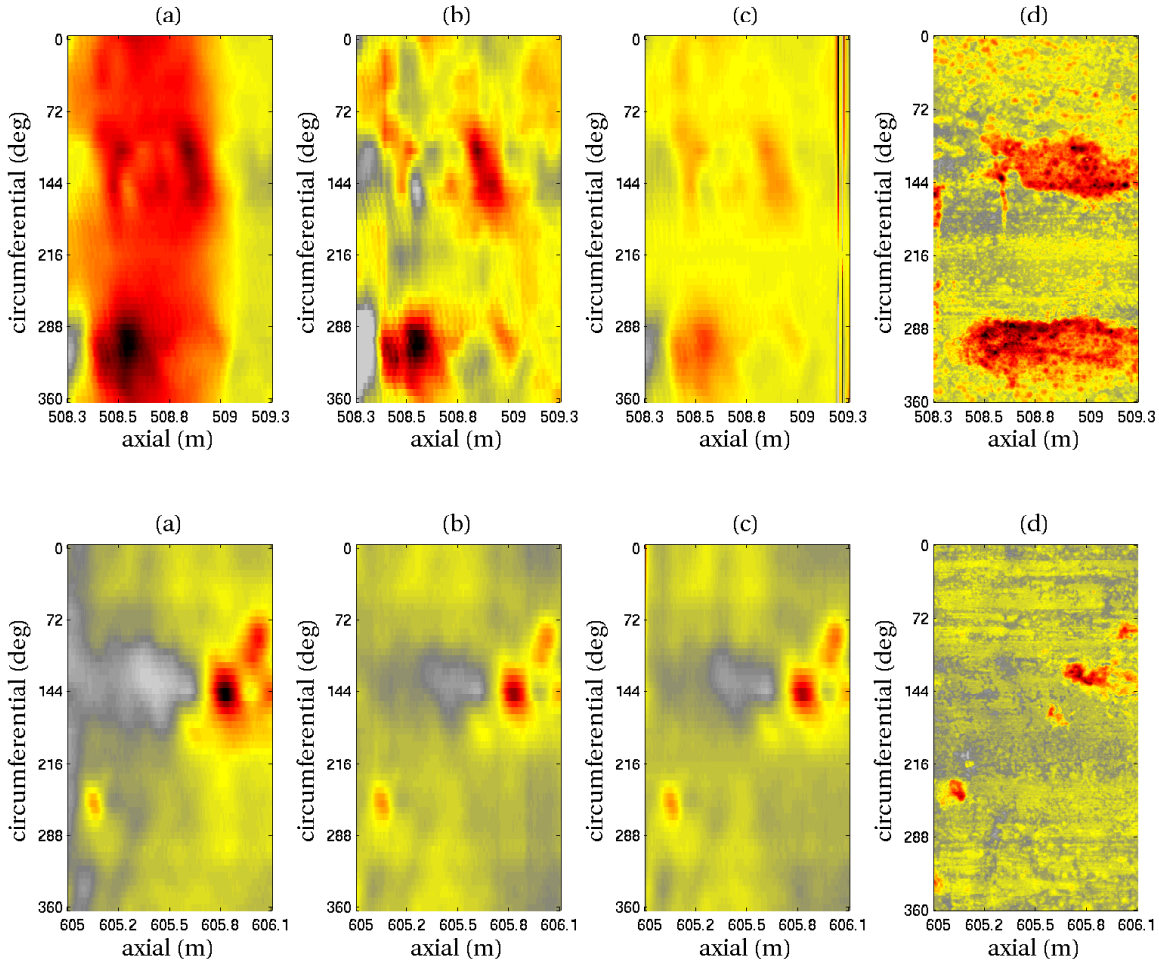

Figure 10: Comparison of different methods to segment and remove the background from the RFEC signal of two pipe segments (top and bottom): (a) raw data (b) proposed method (c) method by Zhang et.al (d) ground-truth

has been extracted. Moreover, our algorithm does not required a manual selection of the sensor lines from the background as Zhang's approach do and it performs better as shown in the results presented in Table 1 and in Figure 10 for the two of the three pipe segments. Note also that Zhang's approach shows a lack of stability (the stripes at the top-right corner of Figure 10b are artefacts of this method).

6 Conclusions

Using a simulation based on the finite element analysis of the RFEC technology, we have provided a qualitative insight on the behaviour of the magnetic field. We have analysed the influence of the pipe's geometry in the exciter coil area. This influence is shown to behave as a circumferential offset and can be describe as a part of the "background of the signal".

In addition, we proposed an automatic method to remove the background component of the signal based on the modification of a standard graph-based segmentation method. The modification of this method increases the sensitivity of the segmentation along the circumferential direction. We validated our approach on a controlled environment generated with a 3D FEA simulation, as well as on a real dataset acquired with a RFEC tool associated with a 3D profile of the pipe.

7 Acknowledgement

This publication is an outcome from the Critical Pipes Project funded by Sydney Water Corporation, Water Research Foundation of the USA, Melbourne Water, Water Corporation (WA), UK Water Industry Research Ltd, South Australia Water Corporation, South East Water, Hunter Water Corporation, City West Water, Monash University, University of Technology Sydney and University of Newcastle. The research partners are Monash University (lead), University of Technology Sydney and University of Newcastle.

References

[Atherton and Czura, 1991] David L Atherton and W Czura. Finite element poynting vector calculation for remote field eddy current inspection of tubes with circumferential slots. *IEEE Transactions on Magnetics*, 27(5):3920–3922, 1991.

[Atherton *et al.*, 1989] David L Atherton, W Czura, Thomas R Schmidt, S Sullivan, C Toal, and T O R Coil. Use of Magnetically-Saturated Regions in Remote Field Eddy Current Tools. *Journal of Nondestructive Evaluation*, 8(1):37–43, 1989.

[Atherton, 1995] David L Atherton. Remote field eddy current inspection. *IEEE Transactions on Magnetics*, 31(6):4142–4147, 1995.

[Bracken and Johnston, 2009] M. Bracken and D. Johnston. Acoustic Methods for Determining Remaining Pipe Wall Thickness in Asbestos Cement, and Ferrous Pipes. *Procs of Pipelines*, pages 271–281, 2009.

[Cardelli *et al.*, 1993] E Cardelli, N Esposito, and M Raugi. Electromagnetic Analysis of RFEC Differential Probes. *IEEE Transactions on Magnetics*, 29(2):1849–1852, 1993.

[Douillard *et al.*, 2012] B Douillard, S Williams, C Roman, O Pizarro, I Vaughn, and G Inglis. FFT-based Terrain Segmentation for Underwater Mapping. In *Robotics: Science and Systems*, 2012.

[Edwards and Palmer, B, 1986] C Edwards and S Palmer, B. The magnetic leakage field of surface-breaking cracks. *Journal of Physics D: Applied Physics*, 19(4):657, 1986.

[Felzenszwalb and Huttenlocher, 2004] Pedro F Felzenszwalb and Daniel P Huttenlocher. Efficient Graph-Based Image Segmentation. *International Journal of Computer Vision*, 59(2):1–26, 2004.

[Lord *et al.*, 1988] W. Lord, Yu Shi Sun, S.S. Udpa, and S. Nath. A Finite Element Study of the Remote Field Eddy Current Phenomen. *IEEE Transactions on Magnetics*, 24(1):435–438, 1988.

[MacLean, 1951] William R. MacLean. Apparatus for magnetically measuring thinckness of ferrous pipe, 1951.

[Mayo and Tapamo, 2009] Zane Mayo and Jules R Tapamo. Background Subtraction Survey for Highway Surveillance. In *Proc. Annu. Symp. PRASA*, pages 77–82, 2009.

[Nakata *et al.*, 1990] T. Nakata, N. Takahashi, K. Fujiwara, and M. Sakaguchi. 3-D Open Boundary Magnetic field Analysis Using Infinite Element Based on Hybrid Finite Element Method. *IEEE Transactions on Magnetics*, 26(2):368–370, 1990.

[Pasadas *et al.*, 2013] Dário J Pasadas, Tiago J Rocha, Helena G Ramos, and A Lopes Ribeiro. Remote Field Eddy Current Inspection of Metallic Tubes Using GMR Sensors. *Instrumentation and Measurement Technology Conference (I2MTC)*, pages 296–299, 2013.

[Peng *et al.*, 2013] Bo Peng, Lei Zhang, and David Zhang. A survey of graph theoretical approaches to image segmentation. *Pattern Recognition*, 46(3):1020–1038, 2013.

[Schmidt, 1989] Thomas R Schmidt. History of the remote-field eddy-current inspection technique. *Materials evaluation*, 42(1):14–22, 1989.

[Skinner *et al.*, 2014] Bradley Skinner, Teresa Vidal-Calleja, Jaime Valls Miro, Freek De Bruijn, and Raphael Falque. 3D Point Cloud Upsampling for Accurate Reconstruction of Dense 2.5D Thickness Maps. In *Proceedings of the Australasian Conference on Robotics and Automation (ACRA)*, Melbourne, AU, Dec 2014.

[Stratton, 2007] Julius Adams Stratton. *Electromagnetic theory*. John Wiley \& Sons, 2007.

[Wu *et al.*, 2009] De-hui Wu, Song-ling Huang, Wei Zhao, and Hong-qing Liu. Research on 3-D Simulation of Remote Fireld Eddy Current Detection for Pipeline Cracks. *Journal of System Simulation*, 21(20):6626–6633, 2009.

[Zhang, 1997] Yanjing Zhang. *Electric and magnetic contributions and defect interactions in remote field eddy current techniques*. PhD thesis, Queen's University, 1997.